

Vanishing conductivity-like Gilbert damping in mirror-symmetric van der Waals ferromagnets

Weizhao Chen,^{1,2,3} Yu Zhang,¹ Yi Liu,^{4,*} and Zhe Yuan^{2,3,†}

¹*Center for Advanced Quantum Studies and School of Physics and Astronomy,
Beijing Normal University, Beijing 100875, China*

²*Institute for Nanoelectronic Devices and Quantum Computing, Fudan University, Shanghai 200433, China*

³*Interdisciplinary Center for Theoretical Physics and Information Sciences, Fudan University, Shanghai 200433, China*

⁴*Institute for Quantum Science and Technology, Department of Physics, Shanghai University, Shanghai 200444, China*
(Dated: November 20, 2024)

The identification of two-dimensional van der Waals ferromagnetic materials has significantly expanded the realm of magnetic materials and enabled innovative control techniques such as gating and stacking. The dynamical behavior of magnetization is profoundly influenced by the Gilbert damping parameter, a crucial factor for enhancing the speed of magnetic switching and reducing the energy consumption of magnetic devices. Despite its importance, the understanding of Gilbert damping in van der Waals ferromagnets remains limited, impeding their technological applications. Here we present a theoretical calculation of Gilbert damping in two-dimensional van der Waals metals, focusing on Fe_3GaTe_2 and Fe_3GeTe_2 as model systems. We discover that mirror symmetry prohibits intraband contributions, resulting in disappearance of conductivity-like damping. Consequently, at low temperatures, the Gilbert damping in single-layer Fe_3GaTe_2 and Fe_3GeTe_2 is remarkably low when the magnetization is perpendicular to the atomic layer, but it increases substantially when the magnetization is reoriented into the atomic plane. Furthermore, topological nodal lines, also protected by mirror symmetry, contribute significantly to damping mediated by interband transitions and can be effectively modulated by adjusting the Fermi level. Our findings elucidate the distinctive characteristics of Gilbert damping in two-dimensional van der Waals ferromagnets, providing valuable insights for the design and optimization of low-dimensional spintronic devices.

Introduction.—The discovery of two-dimensional (2D) van der Waals (vdW) ferromagnetic (FM) materials, exemplified by CrI_3 [1], $\text{Cr}_2\text{Ge}_2\text{Te}_6$ [2], and Fe_3GeTe_2 [3, 4], has not only dramatically broadened the horizon of FM materials but also ignited promising prospects for low-dimensional spintronics devices [5, 6]. This promise stems partly from the fact that magnetism in 2D vdW FM metals can be easily controlled through various flexible approaches [7, 8]. As a typical 2D FM metal, Fe_3GeTe_2 has attracted considerable attention for its spin-orbit torque-driven magnetization switching [9–11], its unconventional tunability in magnetic tunnel junctions [12, 13] and its potential in novel electronic applications [14]. A very similar vdW FM metal Fe_3GaTe_2 [15] has been discovered with an almost identical lattice structure to Fe_3GeTe_2 , yet it boasts a Curie temperature above room temperature, rendering it an ideal candidate for integration into magnetic heterostructures and devices that operate under ambient conditions [16–19].

The quest for designing high-performance memory and logic devices based on 2D vdW FM materials necessitates a profound understanding of the dynamical properties of 2D magnetism [20], particularly how dimensional reduction affects magnetization dynamics in these materials. Gilbert damping, a pivotal parameter in magnetization dynamics [21], dictates the critical current density for current-induced magnetization switching [22], the switching time scale [23] and the velocity of magnetic texture driven by magnetic fields and/or electric currents [24, 25]. In FM transition metals and

alloys, such as Fe, Co, Ni [26–28], FePd [29, 30] and CoFeB [31–33], the experimentally measured damping exhibits non-monotonic temperature dependence. This behavior is well-understood as the superposition of a *conductivity-like* component that decreases with temperature and a *resistivity-like* contribution increasing with temperature. These two components dominate in the low- and high-temperature regimes, respectively. However, in the recently discovered 2D FM metals, Fe_3GeTe_2 and Fe_3GaTe_2 , only the resistivity-like damping has been observed in the limited experimental [34] and theoretical studies [35]. Furthermore, significant damping anisotropy has also been identified in these 2D FM metals [35, 36], suggesting an atypical magnetization relaxation likely stemming from their low-dimensional lattice structures.

In this article, we present a theoretical calculation of the Gilbert damping in 2D vdW FM metals, with a focus on Fe_3GaTe_2 and Fe_3GeTe_2 , based on the first-principles electronic structures. We reveal that the mirror symmetry in these vdW systems precludes the intraband transitions, leading to the absence of conductivity-like damping. Furthermore, the symmetry-protected nodal lines near the Fermi level substantially enhance interband transitions, thereby amplifying the resistivity-like damping. Our findings predict a pronounced anisotropy in Gilbert damping when mirror symmetry is broken by rotating the magnetization from an out-of-plane to an in-plane orientation.

Theoretical methods.—We utilize the torque-

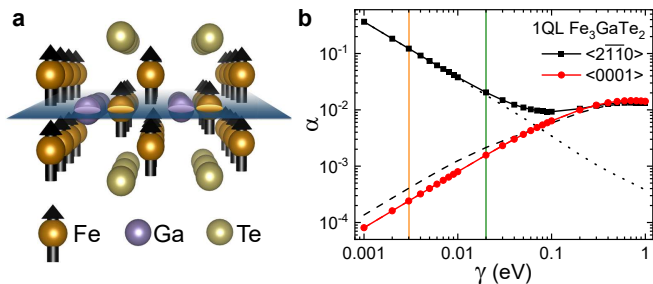


FIG. 1. (a) Schematic representation of the atomic structure of 1QL Fe_3GaTe_2 . The magnetic moments on the Fe atoms are indicated by black arrows. The blue plane in the middle of the layer highlights the mirror symmetry of the lattice structure. (b) Gilbert damping as a function of the electronic scattering rate for 1QL Fe_3GaTe_2 with the out-of-plane (red solid circles) and in-plane magnetization (black solid squares). The dotted and dashed lines represent the contributions from intraband and interband transitions to the damping, respectively. The orange and green vertical lines denote two characteristic scattering rates, $\gamma = 3$ meV and 20 meV, which are used to calculate the damping in detail.

correlation model, as established in literature [37–39], to calculate the Gilbert damping of 2D vdW FM metals based upon first-principles electronic structure. The damping parameter, expressed as a dimensionless quantity, is given by

$$\alpha = \frac{\pi g \mu_B}{M_s} \sum_{n,m} \int \frac{d^3k}{(2\pi)^3} |\Gamma_{mn}^-(\mathbf{k})|^2 \int d\epsilon \eta(\epsilon) A_{n\mathbf{k}}(\epsilon) A_{m\mathbf{k}}(\epsilon). \quad (1)$$

Here g , μ_B and M_s are the Landé factor, the Bohr magneton and the saturation magnetization, respectively. While indices n and m run over all energy bands, the energy derivative of the Fermi-Dirac distribution $\eta(\epsilon) \equiv -\partial f / \partial \epsilon$ highlights that the damping is predominantly influenced by electronic states in the vicinity of the Fermi surface. The matrix element $\Gamma_{mn}^-(\mathbf{k}) = \langle \Psi_{m\mathbf{k}} | [\sigma^-, H_{\text{soc}}] | \Psi_{n\mathbf{k}} \rangle$ characterizes the torque on electron spin stemming from spin-orbit coupling (SOC). The spectral function $A_{n\mathbf{k}}(\epsilon)$ is modeled as a Lorentzian centered at the band energy $\epsilon_{n\mathbf{k}}$, with its width determined by the electronic scattering rate γ [38, 39]. Prior studies have shown that intraband ($n = m$) transitions yield a conductivity-like damping component, which is proportional to the electronic relaxation time, $\tau = \hbar/2\gamma$ [37, 38], while interband ($n \neq m$) transitions contribute to a resistivity-like damping component that scales monotonically with increasing γ [40]. To explicitly evaluate these intraband and interband transitions in Eq. (1), we have developed a Wannier interpolation method to perform the integral of $\Gamma_{mn}^-(\mathbf{k})$ based on the first-principles electronic structures. The self-consistent band structures are calculated using Quantum ESPRESSO [41], and the Wannier functions are constructed using WANNIER90 [42].

Intraband transitions.—The lattice structure of a single layer Fe_3GaTe_2 , referred to as one quintuple-layer (1QL), is depicted in Fig. 1(a). This lattice, belonging to the D_{3h} point group, maintains mirror symmetry about the blue plane only when the magnetization is perpendicular to the atomic plane [15]. The Gilbert damping α of 1QL Fe_3GaTe_2 , calculated using Eq. (1), is plotted in Fig. 1(b) as a function of electronic scattering rate γ . With out-of-plane magnetization ($\mathbf{m} \parallel \langle 0001 \rangle$), α increases monotonically with increasing γ . Detailed analysis shows that the intraband transitions are completely absent, leading to vanishing conductivity-like behavior. In contrast, for in-plane magnetization ($\mathbf{m} \parallel \langle 2\bar{1}10 \rangle$), α exhibits a nonmonotonic dependence on γ , with both conductivity-like and resistivity-like terms contributing. Notably, the significant variation in conductivity-like damping at low scattering rates suggests that a substantial anisotropy in Gilbert damping can be achieved by rotating the magnetization.

The absence of conductivity-like damping with out-of-plane magnetization can be explained through a symmetry analysis of the electronic states. We define \mathcal{M}_z as the mirror operator [43] about the central plane of the 1QL Fe_3GaTe_2 . For $\mathbf{m} \parallel \langle 0001 \rangle$, the system is mirror-symmetric, and thus \mathcal{M}_z commutes with the total Hamiltonian, as well as the SOC Hamiltonian H_{soc} [43]. Consequently, each Bloch state $\Psi_{n\mathbf{k}}$ of the system is an eigenfunction of \mathcal{M}_z with eigenvalues $a_{n\mathbf{k}} = -i$ (symmetric) or $+i$ (antisymmetric). These mirror symmetry properties of Bloch states for 1QL Fe_3GaTe_2 are explicitly calculated using the IRVSP code [44], as shown in Fig. 2(a), where red and blue lines represent symmetric and antisymmetric energy bands with out-of-plane magnetization. Since \mathcal{M}_z anti-commutes with σ^- , we have $\{\mathcal{M}_z, [\sigma^-, H_{\text{soc}}]\} = 0$. Considering the mirror symmetry properties of Bloch states, we find

$$\Gamma_{mn}^-(\mathbf{k}) = -a_{m\mathbf{k}}^* a_{n\mathbf{k}} \Gamma_{mn}^-(\mathbf{k}). \quad (2)$$

For intraband transitions ($m = n$), $|a_{n\mathbf{k}}|^2 = 1$ always holds, leading to $\Gamma_{nn}^-(\mathbf{k}) = -\Gamma_{nn}^-(\mathbf{k})$. This results in $\Gamma_{nn}^-(\mathbf{k}) = 0$ indicating that the intraband transitions are completely forbidden, regardless of the symmetry of the Bloch states. Consequently, the conductivity-like damping vanishes.

Alternatively, the vanishing conductivity-like damping can be intuitively understood by examining the energy dissipation during magnetization dynamics within Kamberský’s breathing Fermi surface model [37, 40]. When the magnetization is out-of-plane at equilibrium, the transverse (in-plane) components of the spin angular momentum $\Delta \mathbf{S}$ relax, as illustrated in Fig. 2(b). The energy of every Bloch state changes with the spin variation $\Delta \mathbf{S}$ through the SOC, i.e., $\Delta \epsilon_{n\mathbf{k}} = \langle \Delta H_{\text{soc}} \rangle_{n\mathbf{k}} \propto \langle \mathbf{L} \rangle_{n\mathbf{k}} \cdot \Delta \mathbf{S}$. Due to the mirror symmetry, the orbital angular momentum must have the same out-of-plane component but opposite in-plane components on either side of the

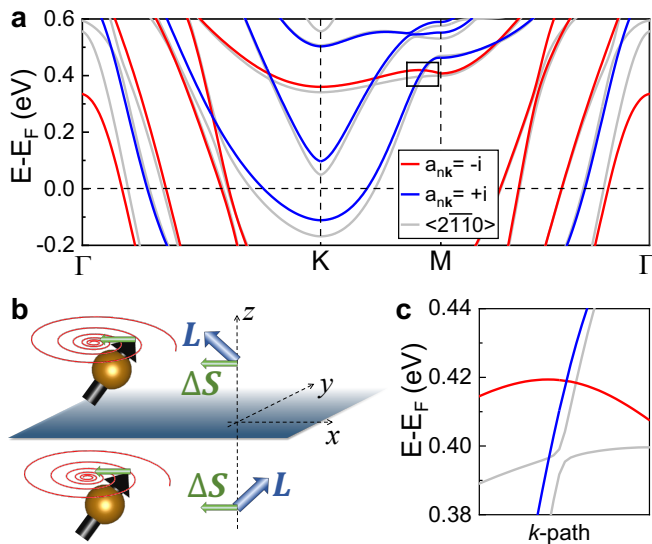


FIG. 2. (a) Calculated band structure of 1QL Fe_3GaTe_2 with out-of-plane magnetization. The red and blue lines denote mirror-symmetric ($a_{n\mathbf{k}} = -i$) and antisymmetric ($a_{n\mathbf{k}} = +i$) bands, respectively. Bands calculated with in-plane magnetization are presented in gray. (b) Schematic illustration of energy dissipation during magnetization dynamics in a mirror-symmetric system. (c) Enlarged view of a typical symmetry-protected band crossing, as indicated by the rectangle in panel (a).

mirror plane, namely $L_z(z) = L_z(-z)$ and $L_{x,y}(z) = -L_{x,y}(-z)$. Therefore, after integrating over the entire space, the band energy remains unchanged with relaxation of the in-plane spin angular momentum, $\Delta\epsilon_{n\mathbf{k}} = 0$. This implies that the breathing Fermi surface during the magnetization dynamics does not excite or dissipate the band energy. Consequently, the conductivity-like damping is absent.

To further confirm that the vanishing conductivity-like damping is indeed a result of symmetry, we intentionally break the mirror symmetry in two distinct ways. First, we gradually rotate the magnetization of 1QL Fe_3GaTe_2 away from the surface normal. This rotation means the Bloch states are no longer eigenstates of \mathcal{M}_z . The calculated energy bands for in-plane magnetization are plotted with gray lines in Fig. 2(a), where the hybridization of the red and blue bands forms anticrossing gaps. A typical example of the energy bands is shown in the zoomed-in plot in Fig. 2(c). Such hybridization of energy bands facilitates intraband transitions, leading to the emergence of the conductivity-like damping, corresponding to the black squares in Fig. 1(b). We select two scattering rates, $\gamma = 3$ meV and 20 meV, as marked by the vertical lines in Fig. 1(b), and calculate damping as a function of the tilting angle θ . As shown in Fig. 3(a), the calculated α increases monotonically with θ and tends to saturate at $\theta > 60^\circ$. The saturation suggests that the energy bands hybridization is strong enough to no longer be treated

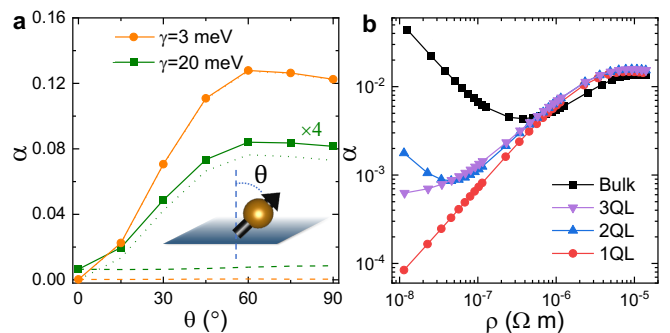


FIG. 3. (a) Gilbert damping for 1QL Fe_3GaTe_2 as a function of the tilting angle θ of the magnetization away from the surface normal, for two scattering rates $\gamma = 3$ meV and 20 meV. The intraband and interband contributions to the damping are represented by dotted and dashed curves, respectively. (b) Gilbert damping for Fe_3GaTe_2 with varying stacking layers plotted as a function of electric resistivity.

as a perturbation. The enhanced damping is dominated by the intraband transitions (the dotted lines) for both γ values, while the interband contributions (the dashed lines) remain nearly unchanged.

The second approach involves varying the number of stacking layers of Fe_3GaTe_2 . By analyzing the lattice structures of 1QL, 2QL and 3QL Fe_3GaTe_2 , we find that mirror symmetry is preserved for odd-number stacking layers but broken in the 2QL system. The calculated damping of Fe_3GaTe_2 with different numbers of stacking layers is shown in Fig. 3(b), plotted as a function of the simultaneously calculated electrical resistivity ρ . The resistivity is calculated using the Boltzmann equation within the relaxation time approximation, where ρ is proportional to the scattering rate $\gamma = \hbar/2\tau$. The calculated α for 1QL and 3QL both monotonically increase with ρ , indicating the absence of conductivity-like damping, as expected due to mirror symmetry. In contrast, α of 2QL Fe_3GaTe_2 exhibits a nonmonotonic dependence on ρ with noticeable conductivity-like contributions at low ρ . The calculated α for bulk Fe_3GaTe_2 , shown as the black squares in Fig. 3(b), contains a much larger conductivity-like component. This is because the mirror symmetry is well defined only for the Bloch states with $k_z = 0$ and those k_z located at the boundary plane of the first Brillouin zone [43]. Other electronic states between these special planes are not eigenstates of the mirror operator. Compared with the bulk case, the significantly reduced damping in Fe_3GaTe_2 thin films at low ρ manifests the strong suppression of the intraband transitions and thus the conductivity-like behavior.

Interband transitions.—Although intraband transitions are prohibited by mirror symmetry, Eq. (2) indicates that interband transitions are allowed between Bloch states with contrasting symmetry characteristics, i.e., $a_{m\mathbf{k}} \neq a_{n\mathbf{k}}$. In fact, the mirror symmetry ensures

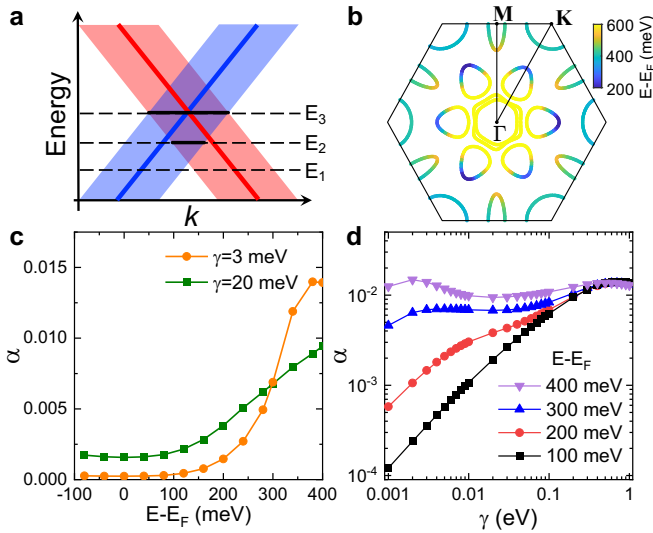


FIG. 4. (a) Schematic representation of the overlap between two broadened energy bands near their crossing point, with shadows indicating the scattering rate-induced broadening. Thick black lines show the extent of overlap at various isoenergetic surfaces. (b) Calculated nodal lines for 1QL Fe_3GaTe_2 with out-of-plane magnetization in the 2D Brillouin zone. (c) Gilbert damping α as a function of energy at two scattering rates. (d) Gilbert damping α as a function of scattering rate at various energy levels.

the presence of nodal lines in the Brillouin zone, which are formed by the intersections of mirror-symmetric and mirror-antisymmetric bands [45, 46]. According to Eq. (1), the interband contribution to damping depends on the overlap of the broadened energy bands at the Fermi energy E_F . As schematically illustrated in Fig. 4(a), the interband contribution from the two intersecting bands is maximized when the intersection point aligns with the Fermi level, i.e., $E_F = E_3$. Consequently, pronounced interband transitions are anticipated near band crossings or nodal lines close to E_F . In the case of 1QL Fe_3GaTe_2 , the nodal lines in the 2D Brillouin zone are predominantly located several hundred meV above E_F , as shown in Fig. 4(b). This accounts for the very low interband damping of 1QL Fe_3GaTe_2 with out-of-plane magnetization, particularly at low γ .

The enhancement of damping by nodal lines is confirmed by elevating E_F in 1QL Fe_3GaTe_2 . Two scattering rates, $\gamma = 3$ meV and 20 meV, were selected, and the calculated damping is plotted in Fig. 4(c) as a function of energy. Near the original E_F , α is minimal and insensitive to energy shifts since the intraband transitions are forbidden and the nodal lines are far above E_F . For $E - E_F > 200$ meV, as energy approaches the nodal lines, α increases rapidly for both γ values due to significantly enhanced interband transitions. We further investigate the scattering rate dependence of α at various energies. As shown in Fig. 4(d), the typical monotonic resistivity-

like damping is observed at $E - E_F = 100$ and 200 meV, where the nodal lines are not significantly involved. In these scenarios, the interband contribution exhibits a nearly linear dependence on γ and tends to saturate at large γ . When scattering occurs at $E - E_F = 300$ and 400 meV, damping becomes substantial even at very low γ . This is because the interband transitions always occur at the crossing point, irrespective of broadening. Thus, the damping displays a very weak dependence on γ . It also implies that the common assumption $\alpha_{\text{interband}} \propto \rho$ does not apply in these instances.

The interband transitions also explain the higher α calculated for 3QL Fe_3GaTe_2 compared to 1QL, as shown in Fig 3(b). With mirror symmetry maintained, we analyze the band structure for 3QL [47]. The tripling of atoms in the unit cell results in a greater number of bands in 3QL compared to 1QL. Consequently, the denser bands in 3QL lead to a significantly larger band overlap under the same broadening γ , culminating in a substantially larger interband contribution to damping for 3QL than for 1QL.

Discussion and conclusion.—Our analysis of the intraband and interband contributions to Gilbert damping reveals an inherent anisotropy in the mirror-symmetric vdW FM material. When the magnetization is oriented out-of-plane, the intraband contribution is symmetry-forbidden, thereby reducing the associated damping. However, by rotating the magnetization into the plane using external fields, the mirror symmetry is broken, leading to the recovery of the intraband (conductivity-like) damping. Consequently, the Gilbert damping can be controlled by adjusting the magnetization orientation without altering the scattering rate. This anisotropic damping is particularly significant in clean systems with relatively low scattering rates, as the intraband contribution is inversely proportional to γ . The calculated damping anisotropy between out-of-plane and in-plane magnetization for Fe_3GaTe_2 is depicted in Fig. 5(a). For both 1QL and 3QL, a substantial anisotropy ratio of up to

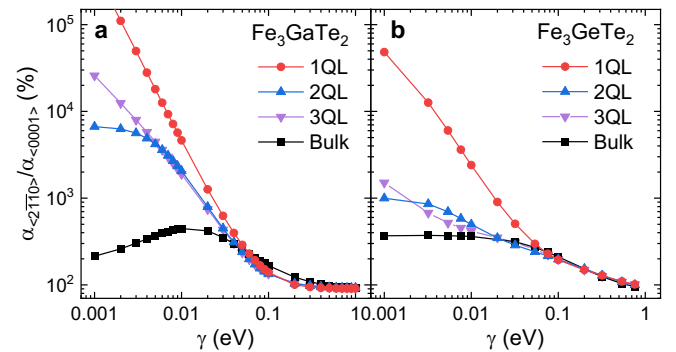


FIG. 5. Calculated damping anisotropy between out-of-plane and in-plane magnetization for Fe_3GaTe_2 (a) and Fe_3GeTe_2 (b).

$10^4\%$ is observed at small γ , and it exceeds 200% for the bulk material. This anisotropy decreases with increasing γ and disappears in the strongly disordered limit, which is governed by interband transitions. The latter depends on the band overlap and is insensitive to symmetry constraint. Fe_3GeTe_2 , which shares the same lattice structure and symmetry as Fe_3GaTe_2 , exhibits the similar properties in its Gilbert damping [47]. Figure 5(b) presents the calculated damping anisotropy of Fe_3GeTe_2 , which is slightly less than that of Fe_3GaTe_2 . This difference arises because the interband contribution is relatively larger in Fe_3GeTe_2 due to the closer proximity of nodal lines to the Fermi level.

In summary, our investigation into the Gilbert damping of 2D vdW ferromagnetic metals, Fe_3GaTe_2 and Fe_3GeTe_2 , has uncovered the role of mirror symmetry in governing the damping behavior. The conductivity-like component of damping in 1QL vanishes under out-of-plane magnetization due to symmetry-prohibited intraband transitions. However, this symmetry can be broken either by tilting the magnetization or by varying the number of layers, which reinstates the intraband contribution and substantially enhances damping. Furthermore, symmetry-protected crossings between mirror-symmetric and antisymmetric bands create nodal lines where the interband transitions are pronounced, leading to a significant damping enhancement. Our findings not only elucidate the microscopic origins of the observed monotonic temperature-dependence of Gilbert damping but also predict an inherent damping anisotropy in these metals that awaits experimental validation. Additionally, we propose that voltage control offers a promising avenue for tuning the damping of Fe_3GeTe_2 and Fe_3GaTe_2 thin films by modulating the Fermi level relative to the nodal lines.

This work was supported by the National Natural Science Foundation of China (Grants No. 12374101 and No. 12174028) and the Open Project of Guangdong Provincial Key Laboratory of Magnetoelectric Physics and Devices, No. 2022B1212010008.

* yiliu42@shu.edu.cn

† yuanz@fudan.edu.cn

- [1] B. Huang, G. Clark, E. Navarro-Moratalla, D. R. Klein, R. Cheng, K. L. Seyler, D. Zhong, E. Schmidgall, M. A. McGuire, D. H. Cobden, W. Yao, D. Xiao, P. Jarillo-Herrero and X. Xu, Layer-dependent ferromagnetism in a van der Waals crystal down to the monolayer limit. *Nature* **546**, 270 (2017).
- [2] C. Gong, L. Li, Z. Li, H. Ji, A. Stern, Y. Xia, T. Cao, W. Bao, C. Wang, Y. Wang, Z. Q. Qiu, R. J. Cava, S. G. Louie, J. Xia and X. Zhang, Discovery of intrinsic ferromagnetism in two-dimensional van der Waals crystals. *Nature* **546**, 265 (2017).
- [3] Z. Fei, B. Huang, P. Malinowski, W. Wang, T. Song, J. Sanchez, W. Yao, D. Xiao, X. Zhu, A. F. May, W. Wu, D. H. Cobden, J.-H. Chu and X. Xu, Two-dimensional itinerant ferromagnetism in atomically thin Fe_3GeTe_2 . *Nat. Mater.* **17**, 778 (2018).
- [4] Y. Deng, Y. Yu, Y. Song, J. Zhang, N. Z. Wang, Z. Sun, Y. Yi, Y. Z. Wu, S. Wu, J. Zhu, J. Wang, X. H. Chen, and Y. Zhang, Gate-tunable room-temperature ferromagnetism in two-dimensional Fe_3GeTe_2 . *Nature* **563**, 94 (2018).
- [5] C. Gong, X. Zhang, Two-dimensional magnetic crystals and emergent heterostructure devices. *Science* **363**, eaav4450 (2019).
- [6] B. Dieny, I. L. Prejbeanu, K. Garello, P. Gambardella, P. Freitas, R. Lehnendorff, W. Raberg, U. Ebels, S. O. Demokritov, J. Akerman, A. Deac, P. Pirro, C. Adelman, A. Anane, A. V. Chumak, A. Hirohata, S. Mangin, S. O. Valenzuela, M. C. Onbasli, M. d'Aquino, G. Prenat, G. Finocchio, L. Lopez-Diaz, R. Chantrell, O. Chubykalo-Fesenko and P. Bortolotti, Opportunities and challenges for spintronics in the microelectronics industry. *Nat. Electronics* **3**, 446 (2020).
- [7] K. S. Burch, D. Mandrus, and J.-G. Park, Magnetism in two-dimensional van der Waals materials. *Nature* **563**, 47 (2018).
- [8] M. Blei, J. L. Lado, Q. Song, D. Dey, O. Erten, V. Pardo, R. Comin, S. Tongay, and A. S. Botana, Synthesis, engineering, and theory of 2D van der Waals magnets. *Appl. Phys. Rev.* **8**, 021301 (2021).
- [9] X. Wang, J. Tang, X. Xia, C. He, J. Zhang, Y. Liu, C. Wan, C. Fang, C. Guo, W. Yang, Y. Guang, X. Zhang, H. Xu, J. Wei, M. Liao, X. Lu, J. Feng, X. Li, Y. Peng, H. Wei, R. Yang, D. Shi, X. Zhang, Z. Han, Z. Zhang, G. Zhang, G. Yu, X. Han, Current-driven magnetization switching in a van der Waals ferromagnet Fe_3GeTe_2 . *Sci. Adv.* **5**, eaaw8904 (2019).
- [10] M. Alghamdi, M. Lohmann, J. Li, P. R. Jothi, Q. Shao, M. Aldosary, T. Su, B. P. T. Fokwa, and J. Shi, Highly efficient spin-orbit torque and switching of layered ferromagnet Fe_3GeTe_2 . *Nano Lett.* **19**, 4400 (2019).
- [11] H. Wang, H. Wu, J. Zhang, Y. Liu, D. Chen, C. Pandey, J. Yin, D. Wei, N. Lei, S. Shi, H. Lu, P. Li, A. Fert, K. L. Wang, T. Nie and W. Zhao, Room temperature energy-efficient spin-orbit torque switching in two-dimensional van der Waals Fe_3GeTe_2 induced by topological insulators. *Nat. Commun.* **14**, 5173 (2023).
- [12] Z. Wang, D. Sapkota, T. Taniguchi, K. Watanabe, D. Mandrus, and A. F. Morpurgo, Tunneling spin valves based on $\text{Fe}_3\text{GeTe}_2/\text{hBN}/\text{Fe}_3\text{GeTe}_2$ van der Waals heterostructures. *Nano Lett.* **18**, 4303 (2018).
- [13] Z.-A. Wang, W. Xue, F. Yan, W. Zhu, Y. Liu, X. Zhang, Z. Wei, K. Chang, Z. Yuan, and K. Wang, Selectively controlled ferromagnets by electric fields in van der Waals ferromagnetic heterojunctions. *Nano Lett.* **23**, 710 (2023).
- [14] J. Xiong, J. Xie, B. Cheng, Y. Dai, X. Cui, L. Wang, Z. Liu, J. Zhou, N. Wang, X. Xu, X. Chen, S.-W. Cheong, S.-J. Liang and F. Miao, Electrical switching of Ising-superconducting nonreciprocity for quantum neuronal transistor. *Nat. Commun.* **15**, 4953 (2024).
- [15] G. Zhang, F. Guo, H. Wu, X. Wen, L. Yang, W. Jin, W. Zhang and H. Chang, Above-room-temperature strong intrinsic ferromagnetism in 2D van der Waals Fe_3GaTe_2 with large perpendicular magnetic anisotropy. *Nat. Commun.* **13**, 5067 (2022).

- [16] H. Pan, C. Zhang, J. Shi, X. Hu, N. Wang, L. An, R. Duan, P. Deb, Z. Liu, and W. Gao, Room-temperature lateral spin valve in graphene/Fe₃GaTe₂ van der Waals heterostructures. *ACS Mater. Lett.* **5**, 2226 (2023).
- [17] W. Jin, G. Zhang, H. Wu, L. Yang, W. Zhang and H. Chang, Room-temperature spin-valve devices based on Fe₃GaTe₂/MoS₂/Fe₃GaTe₂ 2D van der Waals heterojunctions. *Nanoscale* **15**, 5371 (2023).
- [18] Y. Deng, M. Wang, Z. Xiang, K. Zhu, T. Hu, L. Lu, Y. Wang, Y. Ma, B. Lei, X. Chen, Room-temperature highly efficient nonvolatile magnetization switching by current in van der Waals Fe₃GaTe₂ devices. *Nano Lett.* **24**, 9302 (2024).
- [19] Y. Zhang, X. Ren, R. Liu, Z. Chen, X. Wu, J. Pang, W. Wang, G. Lan, K. Watanabe, T. Taniguchi, Y. Shi, G. Yu, Q. Shao, Robust field-free switching using large unconventional spin-orbit torque in an all-van der Waals heterostructure. *Adv. Mater.* **36**, 2406464 (2024).
- [20] C. Tang, L. Alahmed, M. Mahdi, Y. Xiong, J. Inman, N. J. McLaughlin, C. Zollitsch, T. H. Kim, C. R. Du, H. Kurebayashi, E. J. G. Santos, W. Zhang, P. Li, W. Jin, Spin dynamics in van der Waals magnetic systems. *Phys. Rep.* **1032**, 1 (2023).
- [21] T. L. Gilbert, A Phenomenological Theory of Damping in Ferromagnetic Materials. *IEEE Trans. Magn.* **40**, 3443 (2004).
- [22] A. Brataas, A. D. Kent, H. Ohno, Current-induced torques in magnetic materials. *Nat. Mater.* **11**, 372 (2012).
- [23] J. Z. Sun, Spin-current interaction with a monodomain magnetic body: A model study. *Phys. Rev. B* **62**, 570 (2000).
- [24] G. Tatara, H. Kohno, J. Shibata, Microscopic approach to current-driven domain wall dynamics. *Phys. Rep.* **468**, 213 (2008).
- [25] Z. Wang, M. Guo, H.-A. Zhou, L. Zhao, T. Xu, R. Tomasello, H. Bai, Y. Dong, S.-G. Je, W. Chao, H.-S. Han, S. Lee, K.-S. Lee, Y. Yao, W. Han, C. Song, H. Wu, M. Carpentieri, G. Finocchio, M.-Y. Im, S.-Z. Lin and W. Jiang, Thermal generation, manipulation and thermoelectric detection of skyrmions. *Nat Electron* **3**, 672 (2020).
- [26] S. M. Bhagat and P. Lubitz, Temperature variation of ferromagnetic relaxation in the 3d transition metals. *Phys. Rev. B* **10**, 179 (1974).
- [27] B. Heinrich, D. J. Meredith, and J. F. Cochran, Wave number and temperature-dependent Landau-Lifshitz damping in nickel. *J. Appl. Phys.* **50**, 7726 (1979).
- [28] B. Khodadadi, A. Rai, A. Sapkota, A. Srivastava, B. Nepal, Y. Lim, D. A. Smith, C. Memes, S. Budhathoki, A. J. Hauser, M. Gao, J.-F. Li, D. D. Viehland, Z. Jiang, J. J. Heremans, P. V. Balachandran, T. Mewes, and S. Emori, Conductivitylike Gilbert damping due to intraband scattering in epitaxial iron. *Phys. Rev. Lett.* **124**, 157201 (2020).
- [29] D. Zhang, D. Huang, R. J. Wu, D. Lattery, J. Liu, X. Wang, D. B. Gopman, K. A. Mkhoyan, J.-P. Wang, and X. Wang, Low Gilbert damping and high thermal stability of Ru-seeded L1-phase FePd perpendicular magnetic thin films at elevated temperatures. *Appl. Phys. Lett.* **117**, 082405 (2020).
- [30] W. K. Peria, M. B. Katz, J.-P. Wang, P. A. Crowell and D. B. Gopman, Low Gilbert damping and high perpendicular magnetic anisotropy in an Ir-coupled L1₀-FePd-based synthetic antiferromagnet. *Sci. Rep.* **14**, 13290 (2024).
- [31] S. Iihama, S. Mizukami, H. Naganuma, M. Oogane, Y. Ando, and T. Miyazaki, Gilbert damping constants of Ta/CoFeB/MgO(Ta) thin films measured by optical detection of precessional magnetization dynamics. *Phys. Rev. B* **89**, 174416 (2014).
- [32] G. Lu, X. Huang, S. Fan, W. Ling, M. Liu, J. Li, L. Jin, L. Pan, Temperature- and thickness-dependent dynamic magnetic properties of sputtered CoFeB/Ta bilayer films. *Journal of Alloys and Compounds* **753**, 475 (2018).
- [33] R. Mandal, Y. Sasaki, I. Kurniawan, J. Jung, Y. Miura, Y. Sakuraba, K. Hono, and Y. K. Takahashi, Estimation of magnetic Gilbert damping at high temperature: An approach of ferromagnetic resonance study. *ACS Appl. Electron. Mater.* **4**, 4741 (2022).
- [34] J. Zhang, Z. Wang, Z. Li, T. Li, S. Liu, J. Zhang, R.-J. Zhang, Q. Jin, Z. Shi, Y. Liu, Z. Sheng, and Z. Zhang, Sub-THz high spin precession frequency in van der Waals ferromagnet Fe₃GaTe₂. *Nano Lett.* **24**, 12204 (2024).
- [35] P. T. Yang, R. X. Liu, Z. Yuan and Y. Liu, Magnetic damping anisotropy in the two-dimensional van der Waals material Fe₃GeTe₂ from first principles. *Phys. Rev. B* **106**, 134409 (2022).
- [36] L. Alahmed, B. Nepal, J. Macy, W. Zheng, B. Casas, A. Sapkota, N. Jones, A. R. Mazza, M. Brahlek, W. Jin, M. Mahjouri-Samani, S. S.-L. Zhang, C. Mewes, L. Balicas, T. Mewes, and P. Li, Magnetism and spin dynamics in room-temperature van der Waals magnet Fe₃GeTe₂. *2D Mater.* **8**, 045030 (2021).
- [37] V. Kamberský, On the Landau-Lifshitz relaxation in ferromagnetic metals. *Can. J. Phys.* **48**, 2906 (1970).
- [38] K. Gilmore, Y. U. Idzerda, and M. D. Stiles, Identification of the dominant precession-damping mechanism in Fe, Co, and Ni by first-principles calculations. *Phys. Rev. Lett.* **99**, 027204 (2007).
- [39] K. Gilmore, Y. U. Idzerda, and M. D. Stiles, Spin-orbit precession damping in transition metal ferromagnets. *J. Appl. Phys.* **103**, 07D303 (2008).
- [40] V. Kamberský, On ferromagnetic resonance damping in metals. *Czech. J. Phys. B* **28**, 1366 (1976).
- [41] P. Giannozzi *et al.*, Advanced capabilities for materials modelling with Quantum ESPRESSO. *J. Phys.: Condens. Matter* **29**, 465901 (2017).
- [42] G. Pizzi *et al.*, Wannier90 as a community code: new features and applications. *J. Phys.: Condens. Matter* **32**, 165902 (2020).
- [43] F. Zhang, C. L. Kane, and E. J. Mele, Topological mirror superconductivity. *Phys. Rev. Lett.* **111**, 056403 (2013).
- [44] J. Gao, Q. Wu, C. Persson, Z. Wang, Irvsp: To obtain irreducible representations of electronic states in the VASP. *Comput. Phys. Commun.* **261**, 107760 (2021).
- [45] S.-Y. Yang, H. Yang, E. Derunova, S. S. P. Parkin, B. Yan, and M. N. Ali, Symmetry demanded topological nodal-line materials. *Adv. Phys. X* **3**, 1414631 (2018).
- [46] F. L. Zeng, Z. Y. Ren, Y. Li, J. Y. Zeng, M. W. Jia, J. Miao, A. Hoffmann, W. Zhang, Y. Z. Wu, and Z. Yuan, Intrinsic mechanism for anisotropic magnetoresistance and experimental confirmation in Co_xFe_{1-x} single-crystal films. *Phys. Rev. Lett.* **125**, 097201 (2020).
- [47] See Supplemental Material at [URL] for the calculated band structure of 3QL Fe₃GaTe₂, the band structure and Gilbert damping of 1QL Fe₃GeTe₂.